Cystine–glutamate antiporter xCT deficiency suppresses tumor growth while preserving antitumor immunity

Michael D. Arensman[a], Xiaoran S. Yang[a], Danielle M. Leahy[a], Lourdes Toral-Barza[a], Mary Mileski[a], Edward C. Rosfjord[a], Fang Wang[a], Shibing Deng[b], Jeremy S. Myers[a], Robert T. Abraham[b], and Christina H. Eng[a,1]

[a]Oncology Research & Development, Pfizer, Pearl River, NY 10965; and [b]Oncology Research & Development, Pfizer, San Diego, CA 92121

Edited by William G. Kaelin Jr., Dana-Farber Cancer Institute and Brigham and Women's Hospital, Harvard Medical School, Boston, MA, and approved April 2, 2019 (received for review September 1, 2018)

T cell-invigorating cancer immunotherapies have near-curative potential. However, their clinical benefit is currently limited, as only a fraction of patients respond, suggesting that these regimens may benefit from combination with tumor-targeting treatments. As oncogenic progression is accompanied by alterations in metabolic pathways, tumors often become heavily reliant on antioxidant machinery and may be susceptible to increases in oxidative stress. The cystine–glutamate antiporter xCT is frequently overexpressed in cancer and fuels the production of the antioxidant glutathione; thus, tumors prone to redox stress may be selectively vulnerable to xCT disruption. However, systemic inhibition of xCT may compromise antitumor immunity, as xCT is implicated in supporting antigen-induced T cell proliferation. Therefore, we utilized immune-competent murine tumor models to investigate whether cancer cell expression of xCT was required for tumor growth in vivo and if deletion of host xCT impacted antitumor immune responses. Deletion of xCT in tumor cells led to defective cystine uptake, accumulation of reactive oxygen species, and impaired tumor growth, supporting a cancer cell-autonomous role for xCT. In contrast, we observed that, although T cell proliferation in culture was exquisitely dependent on xCT expression, xCT was dispensable for T cell proliferation in vivo and for the generation of primary and memory immune responses to tumors. These findings prompted the combination of tumor cell xCT deletion with the immunotherapeutic agent anti–CTLA-4, which dramatically increased the frequency and durability of antitumor responses. Together, these results identify a metabolic vulnerability specific to tumors and demonstrate that xCT disruption can expand the efficacy of anticancer immunotherapies.

xCT | cystine | cancer | T cells | immunotherapy

The development of T cell-stimulating immunotherapies, such as immune checkpoint blockade (ICB), has led to unprecedented durable responses. However, not all tumor types succumb to treatment, and the response rate even in sensitive tumor types is less than 30% (1–3). Thus, the clinical benefit of anticancer immunotherapies may be expanded if used in combination with therapeutics that target tumor cell-specific vulnerabilities.

Cancer cells are distinguished from normal cells by their oncogene-driven alteration of metabolic pathways (4). A consequence of this metabolic reprogramming is increased production of reactive oxygen species (ROS), which must be countered by endogenous antioxidants to avoid loss of cell viability (5). A key participant in cellular redox homeostasis is xCT (encoded by the *Slc7a11* gene). xCT together with CD98/*Slc3a2* form system x_c^-, which transports cystine (but not cysteine) into the cell in exchange for glutamate export (6, 7). Intracellularly, cystine is reduced to its monomeric form, cysteine, which is important for several cellular processes, including the production of glutathione (GSH), a key intracellular antioxidant. Due to the oxidizing extracellular environment, cystine is more abundant in plasma (and in tissue culture medium) compared with cysteine (8, 9). Thus, tumor cells may rely on xCT to fulfill the majority of their cysteine and GSH needs by importing cystine.

Inhibition of xCT has been investigated as a therapeutic strategy for cancer based on observations that elevated xCT expression on tumor cells correlates with poor prognosis (10–12) and that inhibition of xCT in preclinical studies suppresses tumor growth (10, 12–14). However, these studies relied heavily on the use of sulfasalazine, a clinical compound used for the treatment of rheumatoid arthritis, ulcerative colitis, and Crohn's disease. While sulfasalazine inhibits xCT-mediated uptake of cystine (15), sulfasalazine also inhibits NF-κB (16), sepiapterin reductase (17), and reduced folate carrier (18). Thus, the interpretation of reports attributing sulfasalazine-mediated reductions in tumor growth to xCT inhibition is hampered by the lack of specificity of this drug. Furthermore, immunocompromised mice bearing human tumor xenografts were used to investigate the effects of xCT inhibition in vivo (10, 12–14). While these models provide evidence that tumors rely on xCT for proliferation in vivo, they do not account for the possibility that whole-body xCT inhibition may have deleterious effects on immune responses, potentially undermining the effects of xCT deficiency in tumor cells.

Antigen-specific T cells play critical roles in immunosurveillance and are effectors of tumor cell killing during cancer immunotherapy. Naïve T cells proliferate, differentiate, and acquire effector functions in response to antigenic stimulation of the T cell receptor (TCR) together with costimulatory signals. Upon stimulation, activated human T cells express xCT (19, 20), and their expansion is dependent on adequate concentrations of

Significance

xCT, the cystine–glutamate antiporter, has been implicated in supporting both tumor growth and T cell proliferation; thus, antitumor effects of systemic xCT inhibition may be blunted by compromised antitumor immunity. This report details the unexpected finding that xCT is dispensable for T cell proliferation in vivo and for antitumor immune responses. Consequently, tumor cell xCT loss acts synergistically with the immunotherapeutic agent anti–CTLA-4, laying the foundation for utilizing specific xCT inhibitors clinically to expand the efficacy of existing anticancer immunotherapeutics.

Author contributions: M.D.A., E.C.R., F.W., J.S.M., and C.H.E. designed research; M.D.A., X.S.Y., D.M.L., L.T.-B., M.M., E.C.R., F.W., and C.H.E. performed research; M.D.A., F.W., S.D., R.T.A., and C.H.E. analyzed data; and M.D.A., R.T.A., and C.H.E. wrote the paper.

Conflict of interest statement: All authors are employees and shareholders of Pfizer.

This article is a PNAS Direct Submission.

[1]To whom correspondence should be addressed. Email: christina.eng@pfizer.com.

This article contains supporting information online at www.pnas.org/lookup/suppl/doi:10.1073/pnas.1814932116/-/DCSupplemental.

Published online April 24, 2019.

cystine (19, 21) and the ability to produce GSH (22, 23). Taken together, these findings indirectly support the concept that T cells require xCT in a cell-autonomous fashion for proliferation. If this model is correct, then systemic inhibition of xCT may negatively impact T cell function. Although xCT has been implicated in promoting the pathophysiology of experimental autoimmune encephalomyelitis (EAE), a T cell-driven form of autoimmunity (24, 25), the requirement for xCT in supporting T cell proliferation or antitumor immunity has not been evaluated in vivo.

The effects of xCT loss on tumor cells in immunocompetent models and on antitumor immunity were evaluated by genetically deleting xCT in both murine tumor lines and immunocompetent hosts. Loss of xCT in cancer cells led to ROS accumulation, resulting in decreased tumor growth in vitro and in vivo. Surprisingly, T cell proliferation and antitumor immunity were not impaired in xCT knockout mice, leading us to evaluate the possibility of combining systemic xCT loss with the immunotherapeutic agent anti–CTLA-4. The combination of xCT deletion with anti–CTLA-4 resulted in a remarkable increase in durable responses, suggesting that systemic inhibition of xCT is a viable strategy to expand the efficacy of anticancer immunotherapies.

Results

Loss of xCT Inhibits Tumor Growth. To examine the role of xCT in tumor growth, we generated xCT knockout cell lines by CRISPR-Cas9–mediated targeting of the *Slc7a11* gene followed by expansion of single-cell clones. Murine MC38 colon cancer and Pan02 pancreatic cancer cell lines were selected for gene editing based on their ability to grow in immunocompetent mice. Two MC38 clones (2-1 and 2-6) and two Pan02 clones (1-5 and 1-11) that lacked expression of xCT compared with parental xCT WT cells (Fig. 1*A*) were chosen for additional analysis. The functional loss of xCT was assessed by measuring uptake of radioactively labeled cystine. All $xCT^{-/-}$ clones were deficient in cystine uptake (Fig. 1 *B* and *C*), demonstrating that xCT is the predominant cystine transporter in these cell types. To confirm

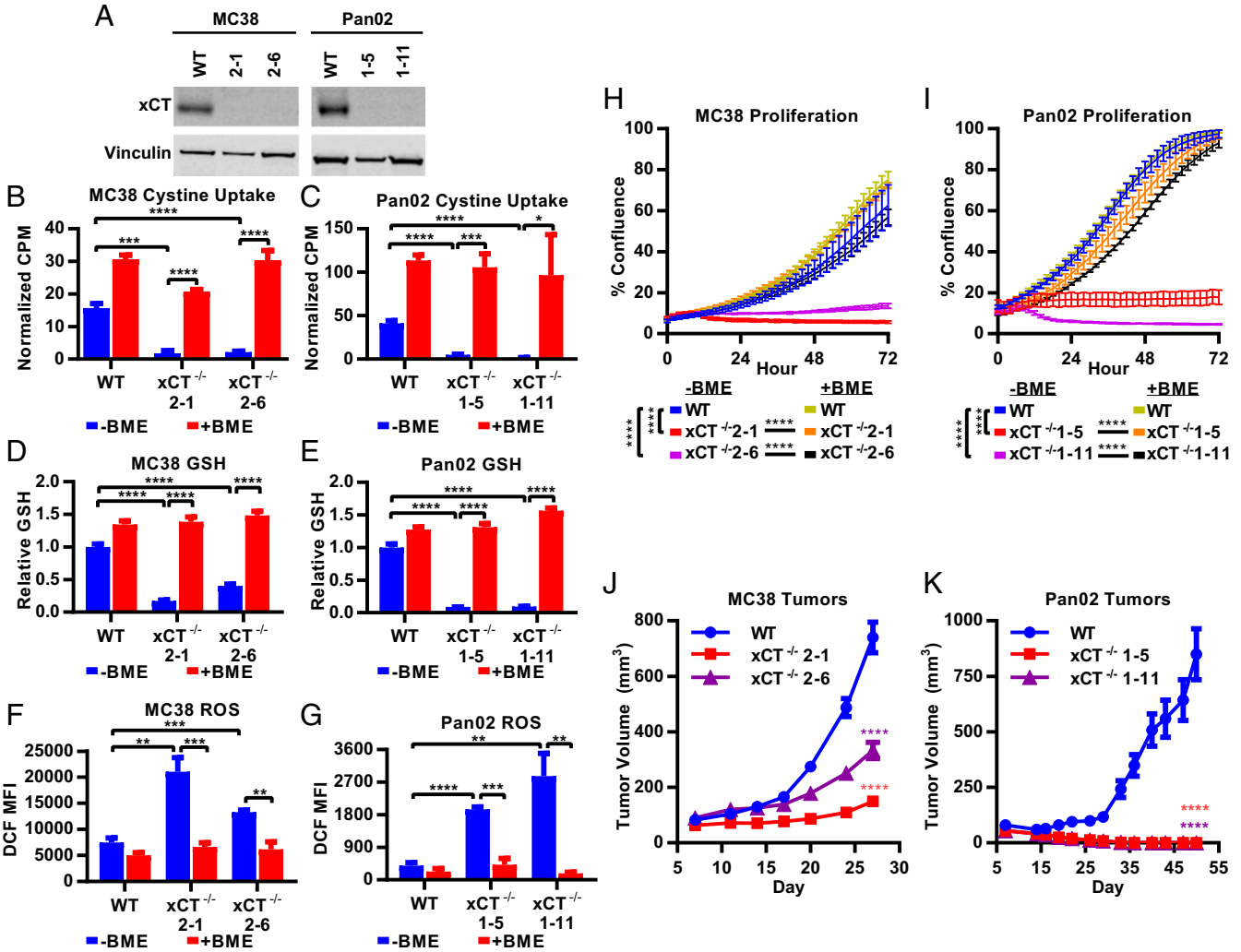

Fig. 1. xCT promotes tumor growth. (*A*) Lysates from MC38 and Pan02 cells probed with anti-xCT or anti-vinculin (loading control) antibodies. (*B* and *C*) ^{14}C-cystine uptake as measured by counts per minute and normalized to CellTiter-Glo (CTG) to account for differences in cell number. (*D* and *E*) Intracellular GSH measured after 7 h in culture by GSH-Glo, normalized to CTG, and shown relative to WT −BME. (*F* and *G*) ROS levels measured after 24 h in culture as indicated by 2′,7′-dichlorodihydrofluorescein diacetate (H_2DCFDA) stain. Cells were first gated on viable singlets. MFI, mean fluorescence intensity. (*H* and *I*) Proliferation was monitored by the IncuCyte imaging system, displayed as percentage confluence, and measured every 2 h. Data represent mean ± SD. One representative experiment from at least three replicates is shown. +BME indicates the addition of 100 μM BME. (*J* and *K*) Tumor cells grown in C57BL/6 mice. Each data point represents the mean tumor volume from at least 15 mice ± SEM. (*B*–*G*) Unpaired two-tailed *t* test. (*H* and *I*) Linear regression analysis. (*J* and *K*) Nonparametric Wilcoxon rank sum test. **P* < 0.05; ***P* < 0.01; ****P* < 0.001; *****P* < 0.0001.

that the deficiency in cystine uptake was due specifically to deletion of xCT, the reducing agent beta-mercaptoethanol (BME) was added to convert the labeled cystine to labeled cysteine. Addition of BME enabled xCT-deficient cells to import cysteine (Fig. 1 *B* and *C*), demonstrating that xCT loss specifically renders cells defective in cystine import. Since cystine import provides free cysteine for the biosynthesis of GSH, a critical antioxidant, GSH and ROS levels were measured in WT and xCT-deficient tumor cells. Loss of xCT in both MC38 and Pan02 cells led to a significant decrease in GSH (Fig. 1 *D* and *E*) and a significant increase in ROS (Fig. 1 *F* and *G*). Both GSH and ROS levels in $xCT^{-/-}$ cells were rescued by the addition of BME (Fig. 1 *D*–*G*), demonstrating that MC38 and Pan02 cells rely on cyst(e)ine import for GSH production and to constrain ROS accumulation.

The impact of xCT loss on tumor cell growth was subsequently evaluated in vitro and in vivo. Both MC38 and Pan02 cell lines displayed dependence on xCT, as deletion of xCT rendered cells unable to proliferate in vitro (Fig. 1 *H* and *I*). Compared with their WT counterparts, xCT-deficient tumor cells exhibited variable but significant decreases in viability, with the exception of Pan02 clone 1-5 (*SI Appendix*, Fig. S1 *A* and *B*). The addition of BME rescued both proliferation and viability of xCT-deficient cells (Fig. 1 *H* and *I* and *SI Appendix*, Fig. S1 *A* and *B*), confirming that the proliferative defect was due to the inability of xCT-deficient cells to import cystine. Next, WT and $xCT^{-/-}$ MC38 and Pan02 tumor cells were engrafted s.c. into C57BL/6 mice. Both xCT-deficient MC38 clones grew significantly slower than WT MC38 tumors in vivo (Fig. 1*J*). The tumor growth defects were even more pronounced in mice engrafted with the Pan02 $xCT^{-/-}$ clones, which failed to maintain measurable tumors after implantation in contrast to their xCT-expressing counterparts (Fig. 1*K*). Thus, the in vivo results were consistent with the in vitro findings, which indicate that xCT supports proliferation in a cancer cell-autonomous fashion.

To confirm that phenotypes observed in the $xCT^{-/-}$ cell lines were specifically due to xCT loss, MC38 and Pan02 cells were transduced with either a lentiviral vector containing Slc7a11 (LvSlc7a11) or a negative control vector (LvNeg). Exogenous xCT could not be detected in Pan02 cells, and therefore, proliferation in the context of xCT reexpression could not be assessed in this cell line. However, MC38 WT and $xCT^{-/-}$ clone 2-1 transduced with LvSlc7a11 had enhanced xCT expression compared with their counterparts transduced with LvNeg (*SI Appendix*, Fig. S1*C*). Reexpressing xCT in the $xCT^{-/-}$ MC38 cell line rescued proliferation in vitro (*SI Appendix*, Fig. S1*D*). When engrafted into C57BL/6 mice, loss of xCT ($xCT^{-/-}$ LvNeg) in MC38 cells reduced tumor burden, resulting in a significant improvement in median survival compared with control cells (WT LvNeg; from 37 to 55 d, log rank $P < 0.0001$). Reexpressing xCT in the knockout cell line ($xCT^{-/-}$ LvSlc7a11) reversed the survival benefit conferred by xCT loss as evidenced by the significant decrease in median survival compared with mice bearing xCT-deficient tumors ($xCT^{-/-}$ LvNeg; from 55 to 43 d, log rank $P < 0.001$) (*SI Appendix*, Fig. S1*E*). Survival was not completely restored to the level of WT LvNeg control cells, likely due to the incomplete restoration of xCT protein (*SI Appendix*, Fig. S1*C*). Furthermore, overexpression of xCT in WT MC38 cells (WT LvSlc7a11) modestly but significantly shortened survival compared with control cells (WT LvNeg; from 37 to 31 d, log rank $P < 0.05$) (*SI Appendix*, Fig. S1*E*), suggesting that enhanced xCT expression results in more aggressive tumors. Taken together, these findings demonstrate that in vitro and in vivo tumor growth defects of the xCT-deficient MC38 cancer cell line are due specifically to loss of xCT protein.

xCT Is Required for T Cell Proliferation in Vitro. Although xCT-mediated cystine uptake supports tumor growth in vivo, cystine is also required for the proliferation of human T cells in vitro (19, 21). Thus, systemic disruption of xCT may negatively impact the immune response against tumors. With the objective of assessing systemic xCT loss in immunocompetent models of cancer, we first set out to determine if stimulated murine T cells exhibit similar cystine dependency and xCT expression as stimulated human T cells (19, 21). Isolated murine splenic T cells were stimulated by CD3/CD28 ligation. Similar to human T cells, murine T cells did not require cystine for activation as measured by cell surface expression of CD25 and CD69 (*SI Appendix*, Fig. S2 *A* and *B*). T cell proliferation was assessed by staining with carboxyfluorescein succinimidyl ester (CFSE) and measurement of dye dilution, which revealed that, analogous to human T cells, murine T cells were completely reliant on cystine for proliferation (*SI Appendix*, Fig. S2*C*). Furthermore, the viability of stimulated murine T cells was severely compromised upon cystine depletion (*SI Appendix*, Fig. S2*D*), and *Slc7a11* mRNA was robustly increased upon stimulation (*SI Appendix*, Fig. S2*E*). Since xCT is expressed upon activation and cystine is required for proliferation, these findings prompted us to evaluate the role of xCT in T cell expansion.

To address the consequences of systemic loss of xCT, C57BL/6 mice with whole-body xCT deficiency were generated by CRISPR-Cas9–mediated targeting of the *Slc7a11* gene. The knockout mice had a 47-bp deletion in exon 1 (*SI Appendix*, Fig. S3*A*), resulting in a premature stop codon and an absence of xCT protein as confirmed by MS in mouse embryonic fibroblasts (MEFs) derived from $xCT^{-/-}$ mice (*SI Appendix*, Fig. S3*B*). Loss of xCT function was confirmed by the impairment of cystine uptake as well as a proliferative defect in $xCT^{-/-}$ MEFs, both of which could be rescued by supplementation with BME (*SI Appendix*, Fig. S3 *C* and *D*). Consistent with previous studies (9), plasma from $xCT^{-/-}$ mice contained comparable levels of cysteine but elevated levels of cystine compared with WT mice (*SI Appendix*, Fig. S3 *E* and *F*), likely due to defective cellular cystine import in vivo.

$xCT^{-/-}$ mice were viable and fertile, and they appeared healthy compared with WT littermates (monitored for up to 1 y). Immune cell profiling was performed on thymuses, spleens, blood, and lymph nodes from WT and $xCT^{-/-}$ mice. Loss of xCT did not alter the distribution of CD4 or CD8 double-negative, double-positive, or single-positive cells, indicating that loss of xCT does not result in gross alterations in T cell development from thymic precursors (*SI Appendix*, Fig. S4*A*). No abnormalities in the ratios of B cells, macrophages, dendritic cells, natural killer cells, T cells, $CD8^+$ T cells, $CD4^+$ helper cells, or Treg cells were observed in $xCT^{-/-}$ mice (*SI Appendix*, Fig. S4*B*). Taken together, these data suggest that xCT is not required for normal lymphoid or myeloid development. Additionally, $xCT^{-/-}$ and WT mice had similar distributions of naïve and memory T cells as evidenced by comparable ratios of $CD62L^{Hi/Lo}$ and $CD44^{Hi/Lo}$ $CD8^+$ and $CD4^+$ T cells (*SI Appendix*, Fig. S4*C*).

As cystine is required for the proliferation but not the activation of stimulated T cells in vitro, we hypothesized that T cells from xCT-deficient mice would have similar phenotypes as cystine-starved T cells. T cells from WT or $xCT^{-/-}$ mice stimulated ex vivo by CD3/CD28 ligation had similar cell surface expression of CD69 and CD25 (Fig. 2 *A* and *B*). $xCT^{-/-}$ T cells were also able to produce IL-2, another indicator of T cell activation, but to a lesser degree than that elaborated by WT T cells (Fig. 2*C*). Similar to our results observed with cystine deprivation, CFSE staining revealed that xCT-deficient T cells were unable to proliferate upon stimulation (Fig. 2*D*), and the viability of $xCT^{-/-}$ T cells was compromised (*SI Appendix*, Fig. S5). Supplementing the medium with BME restored viability (*SI Appendix*, Fig. S5) and proliferative capacity (Fig. 2*D*), demonstrating that T cells depend on xCT to import the cystine required for expansion in vitro.

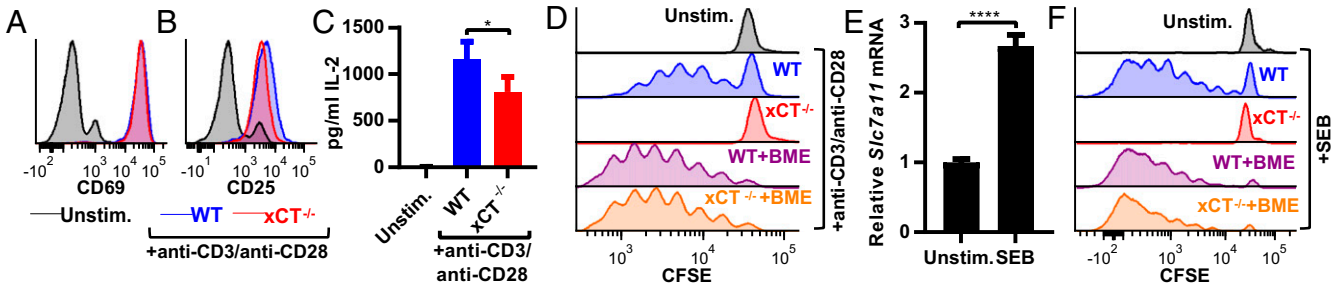

Fig. 2. xCT is required for T cell proliferation in vitro. (*A–D*) Splenic T cells were isolated from WT or xCT$^{-/-}$ mice and stimulated with anti-CD3/anti-CD28 beads. Surface expression of CD69 (*A*) and CD25 (*B*) as measured by flow cytometry 24 h poststimulation. (*C*) IL-2 concentration as measure by ELISA 24 h poststimulation. Error bars represent SD. (*D*) Proliferation of CFSE-stained T cells 3 d poststimulation. T cells were first gated on viable singlets. One representative experiment from at least three replicates is shown. (*E* and *F*) Splenocytes from WT or xCT$^{-/-}$ mice were stimulated with SEB. (*E*) qRT-PCR for *Slc7a11* normalized to *Gapdh* and shown relative to unstimulated (Unstim.) cells 24 h poststimulation. Error bars represent SEM. One representative experiment from two replicates is shown. (*F*) CFSE-stained splenocytes were stimulated with SEB, and flow cytometry was performed 4 d poststimulation. SEB-responsive T cells were identified as singlet, viable, CD3$^+$, and Vβ8$^+$ cells. One representative experiment from at least three independent trials is shown. *$P < 0.05$; ****$P < 0.0001$ (unpaired two-tailed *t* test).

T cells were also stimulated with the superantigen staphylococcal enterotoxin B (SEB), an agent commonly used to provoke T cell proliferation in vivo. Treatment with SEB mimics antigen–TCR engagement by binding MHCII on antigen presenting cells (APCs) and the Vβ8 region of the TCR on T cells. Similar to anti-CD3/anti-CD28–stimulated T cells, SEB-stimulated T cells up-regulated expression of *Slc7a11* mRNA (Fig. 2*E*) and required xCT for proliferation in the absence of BME (Fig. 2*F*). Collectively, these results indicate that murine T cells rely on the xCT-mediated uptake of cystine for proliferation, but not activation, in vitro.

xCT Is Not Required for T Cell Proliferation in Vivo. To determine if xCT is required for the proliferation of stimulated T cells in vivo, we first i.p. injected mice with SEB and analyzed splenic T cells. T cells that encountered SEB in situ up-regulated *Slc7a11* mRNA (Fig. 3*A*) to a similar degree as SEB-stimulated T cells in vitro (Fig. 2*E*). To assess T cell proliferation in vivo, WT or xCT$^{-/-}$ CD45.2$^+$ T cells (from C57BL/6 mice) were labeled with CFSE ex vivo and adoptively transferred to CD45.1 congenic mice to distinguish endogenous from adoptively transferred T cells. In stark contrast to the results seen in vitro, WT and xCT$^{-/-}$ T cells proliferated equally well in vivo after treating the animals with SEB as indicated by CFSE dilution and calculation of the proliferation index (Fig. 3*B*). Furthermore, loss of xCT did not alter the percentage of donor-derived T cells capable of responding to

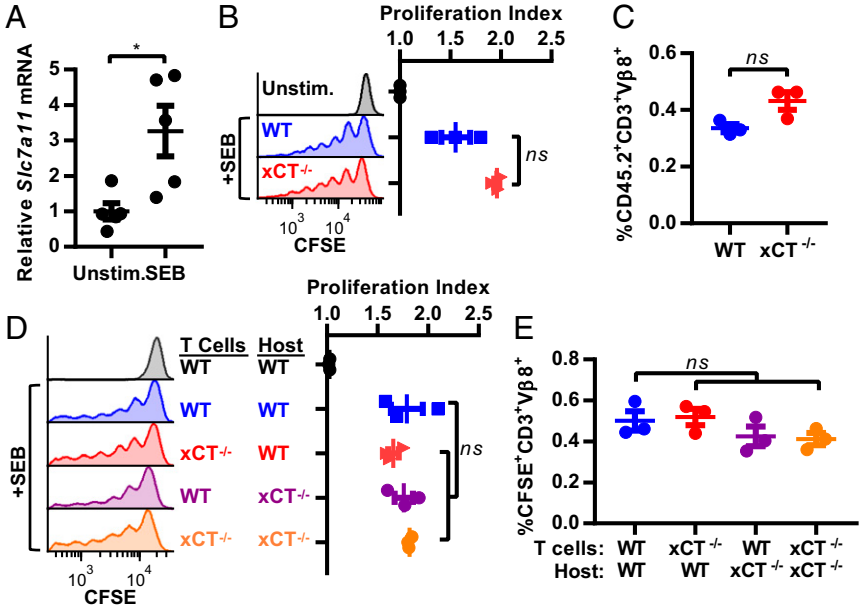

Fig. 3. xCT is not required for T cell proliferation in vivo. Mice were treated with PBS (Unstim.) or SEB. (*A*) RNA was extracted from Vβ8$^+$ splenocytes 24 h posttreatment, and qRT-PCR for *Slc7a11* normalized to *Gapdh* is shown relative to Unstim. Each point represents one mouse ($n = 5$). Error bars represent SEM. One representative experiment from three replicates is shown. (*B* and *C*) CFSE-stained T cells from CD45.2 mice were transferred to CD45.1 mice. Spleens were harvested 3 d posttreatment with SEB. (*B*) Proliferation of donor-derived T cells was measured by CFSE dilution gating on singlets, viable, CD45.2$^+$, CD3$^+$, and Vβ8$^+$ cells. One representative histogram from three mice per group is shown, and the proliferation index for individual mice is shown in *Right*. (*C*) CD45.2$^+$CD3$^+$Vβ8$^+$ (as analyzed in *B*) WT or xCT$^{-/-}$ T cells displayed as a percentage of all viable cells within each spleen of SEB-treated mice. (*D* and *E*) CFSE-stained T cells were transferred to WT or xCT$^{-/-}$ mice, and the mice were treated as in *B*. Cells were gated on singlets, viable, CFSE$^+$, CD3$^+$, and Vβ8$^+$. One representative histogram from three mice per group is shown, and proliferation index for individual mice is shown in *Right*. (*E*) CFSE$^+$CD3$^+$Vβ 8$^+$ (as analyzed in *D*) WT or xCT$^{-/-}$ T cells displayed as a percentage of all viable cells within each spleen of SEB-treated mice. Error bars represent SEM. ns, not significant; *$P <$ 0.05 (unpaired two-tailed *t* test).

SEB (Fig. 3*C*). These results indicate that, although xCT is required for proliferation of T cells in standard tissue culture conditions, xCT is completely dispensable for proliferation of T cells in vivo.

Previous studies have suggested that xCT-expressing APCs import cystine and supply T cells with cysteine in *trans* (26–28). Given that endogenous APCs in CD45.1 mice have the capacity to express xCT, it is plausible that host APCs in the CD45.1 congenic mice rescued the proliferation of transferred xCT-deficient T cells. To rule out this possibility, CFSE-stained WT or xCT$^{-/-}$ T cells were transferred into WT or xCT$^{-/-}$ mice, and T cell expansion was induced with SEB. The presence of CFSE allowed the identification of donor vs. endogenous T cells. In the setting of host xCT deficiency, both WT and xCT$^{-/-}$ T cells proliferated to similar degrees (Fig. 3*D*). There was no significant difference in the proliferation index (Fig. 3*D*) or the percentage of donor T cells able to respond to SEB among the different transplanted T cell groups (Fig. 3*E*). Taken together, these findings demonstrate that xCT is dispensable in both T cells and host tissue for SEB-induced proliferation in vivo.

Loss of xCT Does Not Alter the Antitumor Immune Response. While loss of xCT did not alter SEB-induced T cell proliferation in vivo, we sought to ensure that loss of host xCT did not compromise active antitumor immune responses. In a mouse model of EAE, xCT inhibition with sulfasalazine reduces CD4$^+$ T cell infiltration into the spinal cord (25), suggesting that xCT may also be required for T cell homing to tumors. To ascertain whether xCT loss alters T cell infiltration in tumors, WT MC38 tumor cells were s.c. implanted into WT or xCT$^{-/-}$ mice. Tumors were excised and stained for CD3, CD4, and CD8 by immunohistochemistry (IHC). Tumors from xCT-deficient hosts had similar numbers of infiltrating CD3$^+$, CD8$^+$, and CD4$^+$ cells (Fig. 4*A* and *SI Appendix*, Fig. S6), suggesting that host xCT is not required for T cell migration into tumors.

Another component of the antitumor immune response is the expansion of tumor-reactive T cells. To monitor specific antitumor T cell responses, IFN-γ enzyme-linked immunospot (ELISPOT) assays were performed on splenocytes from naïve or MC38 tumor-bearing WT or xCT$^{-/-}$ mice after ex vivo stimulation with irradiated MC38 tumor cells. Splenocytes from tumor-bearing WT and xCT$^{-/-}$ mice contained a similar number of IFN-γ–secreting cells (Fig. 4*B*), indicating that xCT loss does not impact the generation of tumor reactive T cells.

Although whole-body xCT deletion did not impact T cell homing or tumor reactivity, systemic xCT loss could potentially affect components of the tumor microenvironment that impact tumor infiltrating T cells. To rule out possible confounding effects of systemic xCT loss on T cells, we investigated the consequences of xCT loss specifically in tumor-reactive T cells. OT-I mice express TCRs on CD8$^+$ T cells that specifically recognize an ovalbumin (OVA)-derived peptide presented on MHCI. xCT$^{-/-}$ mice were crossed with OT-I mice to generate xCT-deficient T cells that recognize B16F10 murine tumor cells that express OVA (B16OVA) (29). T cells isolated from these mice were completely dependent on BME for anti-CD3/anti-CD28–induced proliferation in vitro, confirming loss of xCT activity (*SI Appendix*, Fig. S7*A*). Similar to our results with systemic xCT disruption, loss of xCT specifically in tumor-reactive T cells did not hinder the immigration of CD45.2$^+$ OT-I T cells into B16OVA tumors in CD45.1 congenic mice (Fig. 4*C*). The proliferation of adoptively transferred OT-I T cells was also examined. As

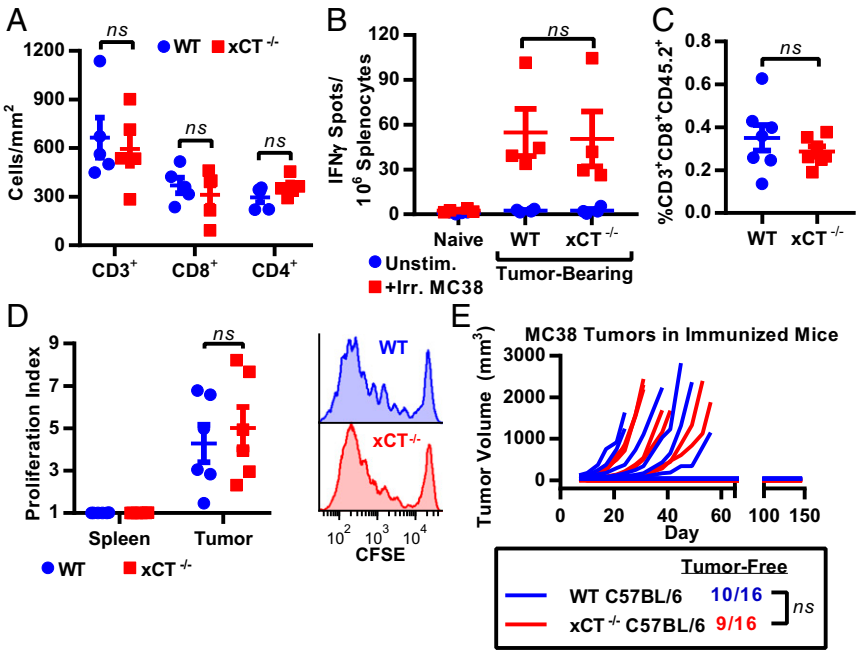

Fig. 4. xCT is dispensable for antitumor immune responses. (*A*) MC38 tumor sections from WT or xCT$^{-/-}$ mice were stained by IHC for CD3$^+$, CD8$^+$, or CD4$^+$ cells and are represented as cells per 1 mm^2 of viable tumor tissue. Each point represents one tumor, and error bars represent SEM. (*B*) IFN-γ ELISPOT performed on spleens from naïve mice or mice bearing WT MC38 tumors. (*C* and *D*) B16OVA tumor-bearing CD45.1 mice received WT or xCT$^{-/-}$ CD45.2$^+$ OT-I T cells. Tissues were collected 4 d posttransfer. (*C*) Tumor-infiltrating WT or xCT$^{-/-}$ OT-I T cells (identified as singlets, viable, CD3$^+$, CD8$^+$, and CD45.2$^+$) displayed as a percentage of all viable cells within each tumor ($n = 7$ mice per group). (*D*) Proliferation index calculated by CFSE dilution of CD45.2$^+$ H-2Kb/SIINFEKL Dextramer$^+$ (OVA-reactive) T cells within spleens or tumors. CD45$^+$ cells were enriched from tumor samples before flow cytometry. Cells were first gated on singlets, viable, CD3$^+$, and CD8$^+$ ($n = 6$ mice per group). Each point represents one mouse, and error bars represent SEM. Representative histograms from tumor-infiltrating OT-I T cells are shown to the right. ns, not significant (unpaired two-tailed *t* test). (*E*) WT or xCT$^{-/-}$ male mice were immunized with irradiated MC38 cells and subsequently challenged with live MC38 cells. Individual tumor growth curves are shown, and number of tumor-free mice is indicated below. ns, not significant (two-sided Fisher's exact test).

anticipated, proliferation of OT-I T cells was not observed in spleens. However, robust proliferation was observed in both WT and xCT$^{-/-}$ OT-I tumor-infiltrating T cells (Fig. 4*D*). Taken together, these findings indicate that neither systemic nor T cell-specific loss of xCT disrupts T cell infiltration or T cell proliferation in response to tumor-associated antigens.

As host xCT was dispensable for the immune response against primary tumors, we next investigated whether host xCT was required for the generation of immunological memory. WT or xCT$^{-/-}$ mice were immunized with irradiated WT MC38 tumor cells and subsequently challenged with live tumors on the opposite flank 3 wk later. Immunization of WT mice with irradiated MC38 tumor cells resulted in tumor rejection, with 63% (10 of 16) of WT mice remaining tumor free 150 d after challenge with live tumors (Fig. 4*E*), Similarly, when xCT$^{-/-}$ mice were immunized with MC38 tumor cells, 56% (9 of 16) of xCT$^{-/-}$ mice remained tumor free 150 d after challenge with live tumors (Fig. 4*E*), demonstrating that both WT and xCT$^{-/-}$ mice are competent to establish and maintain an adaptive immune response against MC38 tumors. Tumors formed in 100% of nonimmunized, WT, and xCT$^{-/-}$ naïve mice after engraftment with MC38 cells, confirming the viability of the implanted tumor cells (*SI Appendix*, Fig. S7*B*).

A similar study was carried out using WT B16OVA tumors. In a preliminary experiment, we demonstrated that B16OVA tumors formed in 100% of naïve mice and grew at similar rates independent of host xCT status (*SI Appendix*, Fig. S7*C*). WT and xCT$^{-/-}$ mice were then immunized with irradiated B16OVA tumor cells and challenged with live B16OVA tumor cells 3 wk later. After 24 d, 60% of WT mice and 60% of xCT$^{-/-}$ mice remained tumor free (*SI Appendix*, Fig. S7*D*), providing additional evidence that WT and xCT$^{-/-}$ mice are equally capable of establishing and maintaining an antitumor immune response.

Given our findings that xCT is dispensable for antitumor immunity, we predicted that host xCT would not suppress the growth of engrafted primary tumors. To determine if host xCT influences tumor growth in vivo, we implanted WT tumor cells into the flanks of WT or xCT$^{-/-}$ mice. Similar to B16OVA tumors (*SI Appendix*, Fig. S7*C*), WT MC38 and Pan02 tumors grew at the same rates in WT and xCT$^{-/-}$ mice (Fig. 5), demonstrating that host xCT has no impact on primary tumor expansion. Furthermore, when xCT$^{-/-}$ tumor cells were engrafted, equally dramatic growth impairments of xCT$^{-/-}$ MC38 tumors occurred in both WT and xCT$^{-/-}$ mice (Fig. 5*A*). Similar results were obtained with xCT$^{-/-}$ Pan02 tumors after engraftment into WT or xCT$^{-/-}$ hosts; however, a small but statistically significant enhancement of xCT$^{-/-}$ Pan02 tumor growth in xCT$^{-/-}$ hosts was observed compared with WT hosts (Fig. 5*B*). Taken together, these data demonstrate that significant tumor growth inhibition is achieved by loss of xCT in the tumor independent of host xCT status.

xCT Loss Enhances Efficacy of Immune Checkpoint Blockade. Our finding that xCT is not required for T cell proliferation in vivo or the establishment of antitumor immunity suggests that systemic targeting of xCT may be advantageously combined with therapies that invigorate antitumor immunity, such as ICB. Blocking the T cell coinhibitory receptor, CTLA-4, with antagonistic antibodies enhances T cell priming and leads to the expansion of antitumor T cells (30). CTLA-4 blockade is thought to stimulate T cells at an earlier stage in the antitumor immune response compared with PD-1/PD-L1 blockade (reviewed in ref. 31). Therefore, anti–CTLA-4 was selected for its potential to stimulate antitumor immunity and to reveal T cell dependencies on xCT.

We first examined whether host xCT modulates responses to anti–CTLA-4 by treating WT and xCT$^{-/-}$ mice bearing WT MC38 tumors with anti–CTLA-4 or IgG control. In line with our findings that xCT is not required for T cell proliferation in vivo, loss of xCT did not significantly alter the levels of proliferative, Ki67-positive tumor-infiltrating T cells (Fig. 6*A*). Although anti–CTLA-4 did not further increase the proliferation of tumor-infiltrating T cells (Fig. 6*A*), anti–CTLA-4 significantly boosted the intratumoral ratio of CD4^{+} T effectors (Teffs) to Treg cells, a positive indicator of anti–CTLA-4 efficacy against tumors (32), in both WT and xCT$^{-/-}$ mice (Fig. 6*B*). Anti–CTLA-4 also enhanced the CD8^{+} to Treg cell ratio in WT and xCT$^{-/-}$ mice, although the increase did not reach statistical significance due to the high intertumoral heterogeneity in the numbers of infiltrating T cells (Fig. 6*C*).

Analogous to our previous results (Fig. 5*A*), MC38 tumors grew equally well in both WT and xCT$^{-/-}$ mice treated with IgG control (Fig. 6 *D* and *E*). When treated with anti–CTLA-4, 27% (4 of 15) of tumor-bearing WT animals had a complete response (CR) (Fig. 6*F*), and median survival was significantly prolonged (from 29 to 45 d, log rank $P < 0.0001$) compared with IgG-treated mice (Fig. 6*L*). Similarly, anti–CTLA-4 treatment resulted in a CR in 33% (5 of 15) of tumor-bearing xCT$^{-/-}$ mice (Fig. 6*G*), which was not significantly different from the CRs observed in anti–CTLA-4–treated WT mice ($P > 0.9999$, Fisher's exact test). Compared with IgG-treated mice, anti–CTLA-4 significantly prolonged the median survival in tumor-bearing xCT$^{-/-}$ mice (from 31 to 43 d, log rank $P = 0.0003$), and there was no significant difference in the median survival rates of WT vs. xCT$^{-/-}$ mice treated with anti–CTLA-4 (45 and 43 d, respectively; log rank $P = 0.7938$) (Fig. 6*L*), demonstrating that anti–CTLA-4 retains its antitumor efficacy even in the absence of host xCT.

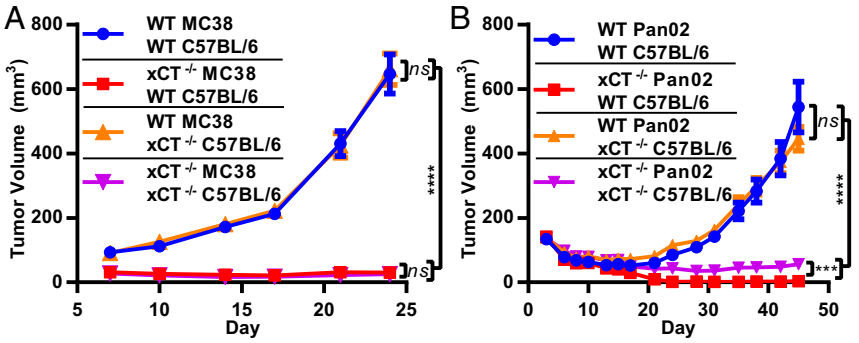

Fig. 5. Host xCT does not impact primary tumor growth. (*A*) WT MC38 or xCT$^{-/-}$ (clone 2-1) or (*B*) WT Pan02 or xCT$^{-/-}$ (clone 1-11) cells were grown in either WT or xCT$^{-/-}$ C57BL/6 mice. Each data point represents the mean from at least 19 mice ± SEM. ns, not significant; ***$P < 0.001$; ****$P < 0.0001$ (nonparametric Wilcoxon rank sum test).

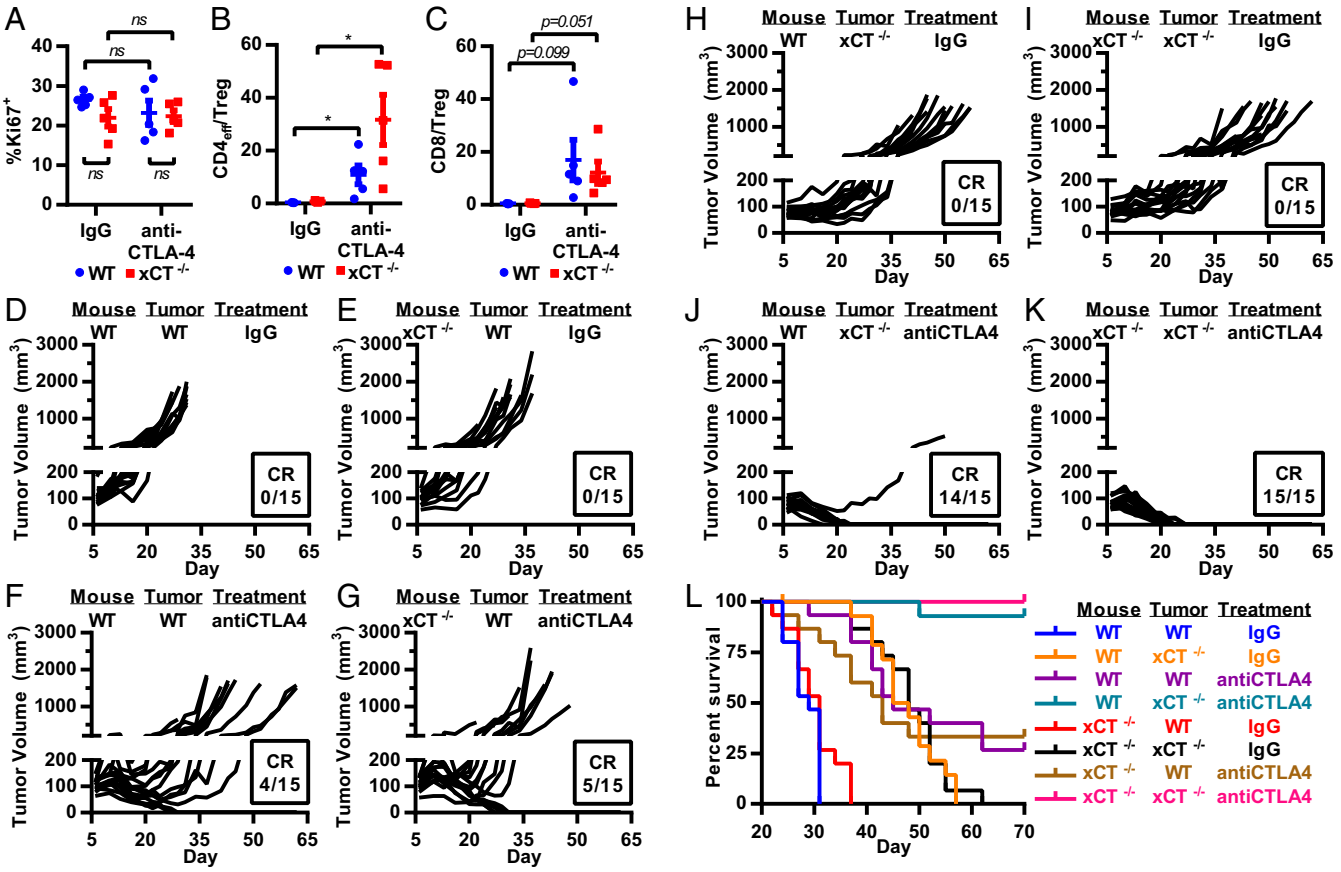

Fig. 6. Tumor cell xCT loss enhances efficacy of anti–CTLA-4. WT or xCT$^{-/-}$ (clone 2-1) MC38 tumor cells were grown as xenografts in WT or xCT$^{-/-}$ mice. Mice were dosed with IgG control or anti–CTLA-4 on days 7, 10, and 13 postimplantation. (*A*–*C*) Flow cytometry on WT MC38 tumors isolated from WT or xCT$^{-/-}$ mice on day 14 postimplantation. (*A*) Ki67 staining of tumor-infiltrating CD3$^+$ T cells. (*B*) CD4$^+$ Teff to Treg cell ratio. Teff = FoxP3$^-$; Treg cell = FoxP3$^+$CD25$^+$. (*C*) CD8$^+$ T cell to Treg cell ratio. Cells were first gated on singlet, viable, CD45$^+$, and CD3$^+$. Each point represents one tumor ($n = 5$). Error bars represent SEM. ns, not significant. *$P < 0.05$ (unpaired two-tailed *t* test). (*D*–*K*) Individual tumor growth curves from each group ($n = 15$). (*L*) Kaplan–Meier survival curves of mice shown in *D*–*K*.

We next evaluated whether loss of xCT in tumor cells enhanced the efficacy of ICB. Consistent with our previous results (*SI Appendix*, Fig. S1*E*), mice bearing xCT$^{-/-}$ tumors displayed significantly improved median survival (47 d) compared with mice with WT tumors (29 d; log rank $P < 0.0001$) (Fig. 6*L*), but all mice developed tumors and eventually succumbed to the disease (Fig. 6*H*). Remarkably, the combination of tumor cell-intrinsic xCT deficiency with CTLA-4 antagonism increased the CRs from 27% (4 of 15) in anti–CTLA-4–treated mice bearing WT tumors (Fig. 6*F*) to 93% (14 of 15) in anti–CTLA-4–treated mice bearing xCT$^{-/-}$ tumors (Fig. 6*J*) ($P = 0.0005$, Fisher's exact test), demonstrating that loss of tumor cell xCT dramatically enhances the efficacy of anti–CTLA-4. Similarly, the efficacy of anti–CTLA-4 in combination with tumor cell xCT loss was preserved in the absence of host xCT [100% CR (15 of 15)] (Fig. 6*K*) and was greater than either tumor cell xCT loss [0% CR (0 of 15)] (Fig. 6*I*) or anti–CTLA-4 [33% CR (5 of 15)] (Fig. 6*G*) alone ($P \leq 0.0002$, Fisher's exact test). Collectively, these data demonstrate that the immune response elicited by anti–CTLA-4 is preserved in the absence of host xCT, and tumor-specific loss of xCT significantly enhances the efficacy of CTLA-4 blockade.

Discussion

Although T cells require GSH for proliferation in vitro and in vivo (22, 23), previous reports have been conflicting as to whether T cells accumulate cysteine directly through xCT-mediated import of cystine (19–21, 33) or indirectly via uptake of cysteine secreted by APCs (26–28). Our results indicate that cystine is necessary and sufficient to support the proliferation of purified T cell cultures in standard culture conditions. Using CRISPR-Cas9 to specifically abrogate xCT expression, we demonstrate that xCT is required for the proliferation of stimulated murine T cells in vitro. Therefore, our findings are in line with previous reports showing that activated human T cells express xCT and import cystine from the extracellular milieu (19–21, 33). Collectively, the results of this study support a T cell-autonomous requirement for xCT function in cultured lymphocytes.

Our discovery that xCT is expendable for T cell proliferation and function in vivo unexpectedly yielded results that clearly conflicted with those obtained ex vivo. Although others have reported that either systemic or immune cell-specific disruption of xCT can alleviate T cell-driven EAE (24, 25), we have found that systemic or T cell-specific knockout of xCT does not disrupt the antitumor T cell response. While we focused on T cell proliferation and the adaptive immune response against tumors, it has also been reported that xCT-deficient mice exhibit enhanced expression of IL-1β and TNF-α at the site of 3-methylcholanthrene injection, which was attributed to increased death of macrophages and neutrophils (34). Therefore, our findings do not exclude the possibility that xCT is required for innate immunity or the resolution of inflammatory responses.

The drastically different requirements for xCT during T cell proliferation in vitro vs. in vivo are likely due to the well-established discrepancies between the tissue culture environment

and the physiologic niches where T cells respond to antigenic stimuli in vivo. For example, T lymphocytes are exposed to much higher levels of oxygen under standard tissue culture conditions than they experience in peripheral tissues in intact organisms (35). Hence, the supraphysiologic oxygen tension in culture medium would increase the pressure on intracellular antioxidants to maintain redox homeostasis in vitro. Additionally, metabolites, such as cysteine, cystine, and GSH, are present at different levels in culture medium vs. plasma and peripheral tissues in vivo. Unless a reducing agent, such as BME, is added, cysteine is absent in cell culture medium, as it is rapidly oxidized to cystine. Although cystine concentrations exceed those of cysteine by approximately twofold in plasma (8), cysteine is nonetheless present at low levels in blood, and therefore, we cannot exclude the possibility that circulating cysteine is sufficient to support T cell proliferation in vivo. Furthermore, cysteine may be present at higher concentrations in specific locations of antigen-induced T cell proliferation, such as tumors and lymph nodes. Specific thiol concentrations in these regions remain undefined due to the technical challenges associated with collecting extracellular fluid within tissues and preventing the oxidation of cysteine during necropsy. However, cysteine and GSH are more abundant in experimental skin blister fluid (a representation of metabolite levels in extracellular fluid surrounding skin cells) than in plasma (36), which supports the possibility that there are additional differences in free thiol levels in plasma vs. tissues where T cells respond to antigen. We, therefore, speculate that the presence of cysteine and other thiols in extracellular fluids obviates the dependence of T cells on xCT in vivo.

The unique dependence of tumor cells on xCT in contrast to the dispensability of xCT in normal tissue may be linked to the level of redox stress associated with tumorigenesis. It has been widely reported that oncogene-transformed cells, including tumor cells, bear increased levels of ROS compared with normal tissues (37–39), which may render tumors hypersensitive to alterations that decrease antioxidant pools, such as the reduction in cystine import caused by loss of xCT. In support of this concept, it has recently been demonstrated that tumors succumb to lethal accumulation of ROS and oxidative DNA damage induced by adoptive immunotherapy (40). These findings could also explain the robust tumor growth inhibition achieved with tumor cell xCT loss in immune-competent mice in the context of CTLA-4 blockade.

We report that loss of xCT in tumor cells prevents growth in vitro and slows tumor progression in vivo. Based on previous reports, it is likely that the absence of xCT impairs stress resistance and reduces viability of tumor cells; notably, xCT inhibition has been shown to trigger oxidative stress-induced autophagic cell death (12), caspase-mediated apoptosis (13), and ferroptosis (41–43), an iron-dependent form of cell death (44). In addition to these mechanisms, the heterogeneous impact of xCT loss on cancer cell viability observed in our study (*SI Appendix*, Fig. S1 *A* and *B*) raises the possibility that xCT disruption may have cytostatic in addition to cytotoxic effects on tumors.

Given our finding that CTLA-4 inhibition leads to the eradication of over 95% of established xCT$^{-/-}$ tumors (Fig. 6 *J* and *K*), it is also tempting to speculate that xCT loss may render tumor cells more immunogenic. Sulfasalazine and erastin, two disparate molecules that inhibit xCT, induce ROS accumulation and endoplasmic reticulum (ER) stress (42). ROS and ER stress mediate the mitoxantrone-induced cell surface exposure of calreticulin (45), a hallmark of immunogenic cell death (46), a process that primes immune cells to attack tumors. These collective observations suggest that, in addition to cell-autonomous effects, xCT loss/inhibition could render tumor cells more immunogenic and more likely to respond to T cell-invigorating immunotherapy. Additional studies are needed to characterize the form(s) of cancer cell death induced by loss of xCT function and how this alteration in tumor tissues impacts antitumor immune responses.

Although the synergy between xCT disruption and CTLA-4 blockade was striking, our studies were carried out primarily in the MC38 tumor cell line. Due to its high mutational burden (47) and partial responsiveness to single-agent ICB (Fig. 6*E*), MC38 cells are considered to be one of the more immunogenic of the commonly used syngeneic murine tumor models. Therefore, it will be important to examine responsiveness to xCT disruption in other less immunogenic tumor models to determine the true extent to which xCT inhibition can expand the population that benefits from ICB therapy.

In conclusion, we have established xCT as a promising therapeutic target for cancer. Specific deletion of xCT in tumor cells robustly decreased tumor burden in murine models of cancer, whereas loss of xCT in host tissues had no positive or negative impact on tumorigenesis. Although genetic knockout experiments in mice may not accurately predict outcomes obtained with drug-induced target inhibition, the phenotypic normalcy of xCT knockout mice and the dispensability for xCT in the antitumor immune response suggest that systemic administration of a specific xCT inhibitor will deliver antitumor efficacy with an acceptable safety profile. We also demonstrated that tumor-specific loss of xCT considerably enhances the efficacy of anti–CTLA-4, suggesting that a therapeutic xCT inhibitor may augment the capacity of checkpoint inhibitor-based immunotherapeutics to extend survival of cancer patients.

Materials and Methods

Cell Culture. MC38 cells were purchased from OBio, and Pan02 cells were obtained from the National Cancer Institute. B16OVA M04 (29) was obtained through a license agreement with Dana-Farber Cancer Institute. MC38 and Pan02 were cultured in DMEM with 10% FBS and penicillin/streptomycin (complete DMEM), and B16OVA M04 was cultured in Iscove's modified Dulbecco's medium (IMDM) + Glutamax with 10% FBS and penicillin/streptomycin at 37 °C in a humidified incubator with 5% CO_2. All cell lines tested negative for mycoplasma throughout the course of the study. Details regarding MEF isolation, generation of xCT-deficient tumor cell lines, proliferation assays, viability assays, cystine uptake assays, ROS quantification, and GSH measurements can be found in *SI Appendix, SI Methods*.

Animals. All procedures performed on animals were in accordance with regulations and established guidelines, and they were reviewed and approved by Pfizer's Institutional Animal Care and Use Committee. All mice were females between the ages of 8–12 wk unless otherwise noted. xCT$^{-/-}$ mice were generated at The Jackson Laboratory by the delivery of CRISPR-Cas9 reagents to mouse zygotes as previously described (48). Slc7a11 knockout alleles were produced by microinjection of in vitro-transcribed guide ribonucleic acid (gRNAs) containing the protospacer sequences 5′-CTCCAGAACACGGGCAGCGT and 5′-AAAAAGTGACAGTACTCCAC. Guide selection was performed with Benchling online software (https://benchling.com/). One-cell zygotes from the C57BL/6J inbred mouse strains (stock JR00664; The Jackson Laboratory) were injected with a microinjection mixture containing the gRNA at 50 ng/μL and synthetic polyadenylated/5-methylcytidine capped Cas9 mRNA (L-6125; TriLink Biotechnologies) at 100 ng/mL. PCR primers (forward 5′-TGGTCAGAAAGCCAGTTGTG and reverse 5′-CCTGCAGGAAGGAATCTGAG) flanking the gRNA target sites were used to amplify the region of interest from founder progeny. PCR amplicons were subsequently processed for Sanger sequencing, which revealed a 47-bp deletion in exon 1 of Slc7a11. Founders with desired indel mutations were bred with C57BL/6J mice to produce N1 progeny that were confirmed by sequence analysis of PCR amplicons using the same primers.

OT-I mice (49) were obtained from The Jackson Laboratory (stock 003831) and maintained as hemizygous for Tg(TcraTcrb) (WT OT-I). Homozygous Slc7a11 knockout female mice were bred with hemizygous OT-I male mice to generate heterozygous Slc7a11/hemizygous OT-I mice. Heterozygous Slc7a11/hemizygous OT-I females were then bred with homozygous Slc7a11 knockout mice to generate homozygous Slc7a11 knockout/hemizygous OT-I (xCT$^{-/-}$ OT-I).

For tumor xenograft studies, 1×10^6 MC38 or 5×10^6 Pan02 cells were suspended in Dulbecco's PBS (DPBS) and s.c. implanted into the hind flanks of mice. IgG control (BP0131) or anti–CTLA-4 (BP0087; Bio X Cell) was administered i.v. at 10 mg/kg on days 7, 10, and 13 postengraftment. Vaccination experiments were performed by first implanting 1×10^6 irradiated (50 Gy) B16OVA M04 or MC38 tumor cells. Three weeks later, 5×10^5 live B16OVA M04 or 1×10^6 live MC38 tumor cells were implanted into the opposite flank, and

tumor take was tallied. Mice were euthanized when tumors ulcerated or when tumors reached 1,500 mm^3. Tumor size was assessed by caliper measurements, and volume was calculated by (width^2 × length)/2.

IHC and Digital Image Analysis. MC38 tumors were harvested 14 d post-engraftment. Briefly, 5-μm tumor sections were deparaffinized, blocked, stained with primary antibodies (*SI Appendix*, Table S1), stained with HRP-conjugated secondary antibodies, and stained in DAB or Vina Green. Slides were then counterstained in hematoxylin and scanned, and Visiopharm software was utilized to quantify chromagen-positive cells. Detailed methods can be found in *SI Appendix, SI Methods*.

T Cell Assays. All assays were performed with freshly isolated T cells from ACK-lysed, manually dissociated spleens using the Mouse Pan T (CD90.2) Kit (11465D; ThermoFisher), and cultured in DMEM (with or without cystine) supplemented with 10% FBS, 1× nonessential amino acids (11140050; ThermoFisher), and antibiotic–antimycotic (15240062; ThermoFisher). Details on in vitro and in vivo T cell proliferation assays can be found in *SI Appendix, SI Methods*.

MS. Briefly, liquid chromatography (LC)-MS/MS was utilized to determine cysteine and cystine concentrations in mouse plasma after *N*-ethylmaleimide treatment of blood obtained via cardiac puncture. Relative quantitation of xCT protein was performed by trypic digestion of proteins isolated from the membrane fraction of MEFs followed by MS. Detailed methods can be found in *SI Appendix, SI Methods*.

Statistics. Unpaired two-tailed *t* tests, two-sided Fisher's exact tests, linear regression analysis, and log-rank tests of Kaplan–Meier survival curves were performed in GraphPad Prism software version 7.04. For IncuCyte experiments, a linear regression model was fit for each group, and slopes (growth rate) of the linear regression from different groups were compared with an *F* test. For xenograft experiments, some animals had unmeasurable tumor (tumor volume = 0 mm^3) in several treatment groups. Therefore, a two-sided nonparametric Wilcoxon rank sum test was performed to compare tumor volumes between two groups at individual time points. No multiple comparison adjustment was applied to the *P* values. Slope analysis was used in *SI Appendix*, Fig. S7 *B* and *C*, because several animals had to be euthanized early in the study due to large tumor size. Under an exponential tumor growth model, the tumor growth rate is the slope of the linear relationship between log tumor size and time. A linear mixed effect model was fit to the growth curve data with a random intercept and a random slope parameter. Comparisons of individual slopes were made between groups under this model with a *t* test. Wilcoxon rank sum tests and slope analyses were performed in R v3.3.3.

Details regarding immunoblotting, qRT-PCR, ELISPOT, and flow cytometry can be found in *SI Appendix, SI Methods*.

ACKNOWLEDGMENTS. We thank the Zhang laboratory from the Broad Institute and McGovern Institute of Brain Research at the Massachusetts Institute of Technology for providing CRISPR reagents, Dan Shao and Shelley Zhang at HD Biosciences for generating xCT$^{-/-}$ tumor cell lines and cystine uptake assays, Katie Tsao and The Jackson Laboratory for generating xCT-deficient mice, Jonathan Golas and Stephanie Bisulco for tissue sectioning and staining, John Kreeger and Alan Opsahl for digital image analysis, Vlad Buklan and Roger Conant for harvesting mouse tissue, and Jessica Kearney and Shirley Markant for generation of MEFs.

1. Hodi FS, et al. (2010) Improved survival with ipilimumab in patients with metastatic melanoma. *N Engl J Med* 363:711–723.
2. Brahmer JR, et al. (2012) Safety and activity of anti-PD-L1 antibody in patients with advanced cancer. *N Engl J Med* 366:2455–2465.
3. Topalian SL, et al. (2012) Safety, activity, and immune correlates of anti-PD-1 antibody in cancer. *N Engl J Med* 366:2443–2454.
4. Pavlova NN, Thompson CB (2016) The emerging hallmarks of cancer metabolism. *Cell Metab* 23:27–47.
5. Reczek CR, Chandel NS (2017) The two faces of reactive oxygen species in cancer. *Annu Rev Cancer Biol* 1:79–98.
6. Bassi MT, et al. (2001) Identification and characterisation of human xCT that co-expresses, with 4F2 heavy chain, the amino acid transport activity system xc-. *Pflugers Arch* 442:286–296.
7. Bannai S, Kitamura E (1980) Transport interaction of L-cystine and L-glutamate in human diploid fibroblasts in culture. *J Biol Chem* 255:2372–2376.
8. Psychogios N, et al. (2011) The human serum metabolome. *PLoS One* 6:e16957.
9. Sato H, et al. (2005) Redox imbalance in cystine/glutamate transporter-deficient mice. *J Biol Chem* 280:37423–37429.
10. Ji X, et al. (2018) xCT (SLC7A11)-mediated metabolic reprogramming promotes non-small cell lung cancer progression. *Oncogene* 37:5007–5019.
11. Yang Y, Yee D (2014) IGF-I regulates redox status in breast cancer cells by activating the amino acid transport molecule xC-. *Cancer Res* 74:2295–2305.
12. Guo W, et al. (2011) Disruption of xCT inhibits cell growth via the ROS/autophagy pathway in hepatocellular carcinoma. *Cancer Lett* 312:55–61.
13. Dai L, Cao Y, Chen Y, Parsons C, Qin Z (2014) Targeting xCT, a cystine-glutamate transporter induces apoptosis and tumor regression for KSHV/HIV-associated lymphoma. *J Hematol Oncol* 7:30.
14. Timmerman LA, et al. (2013) Glutamine sensitivity analysis identifies the xCT antiporter as a common triple-negative breast tumor therapeutic target. *Cancer Cell* 24: 450–465.
15. Gout PW, Buckley AR, Simms CR, Bruchovsky N (2001) Sulfasalazine, a potent suppressor of lymphoma growth by inhibition of the x(c)- cystine transporter: A new action for an old drug. *Leukemia* 15:1633–1640.
16. Wahl C, Liptay S, Adler G, Schmid RM (1998) Sulfasalazine: A potent and specific inhibitor of nuclear factor kappa B. *J Clin Invest* 101:1163–1174.
17. Chidley C, Haruki H, Pedersen MG, Muller E, Johnsson K (2011) A yeast-based screen reveals that sulfasalazine inhibits tetrahydrobiopterin biosynthesis. *Nat Chem Biol* 7: 375–383.
18. Jansen G, et al. (2004) Sulfasalazine is a potent inhibitor of the reduced folate carrier: Implications for combination therapies with methotrexate in rheumatoid arthritis. *Arthritis Rheum* 50:2130–2139.
19. Levring TB, et al. (2012) Activated human CD4+ T cells express transporters for both cysteine and cystine. *Sci Rep* 2:266.
20. Garg SK, Yan Z, Vitvitsky V, Banerjee R (2011) Differential dependence on cysteine from transsulfuration versus transport during T cell activation. *Antioxid Redox Signal* 15:39–47.
21. Levring TB, et al. (2015) Human CD4+ T cells require exogenous cystine for glutathione and DNA synthesis. *Oncotarget* 6:21853–21864.
22. Suthanthiran M, Anderson ME, Sharma VK, Meister A (1990) Glutathione regulates activation-dependent DNA synthesis in highly purified normal human T lymphocytes stimulated via the CD2 and CD3 antigens. *Proc Natl Acad Sci USA* 87:3343–3347.
23. Mak TW, et al. (2017) Glutathione primes T cell metabolism for inflammation. *Immunity* 46:675–689.
24. Merckx E, et al. (2017) Absence of system x_c^- on immune cells invading the central nervous system alleviates experimental autoimmune encephalitis. *J Neuroinflammation* 14:9.
25. Evonuk KS, et al. (2015) Inhibition of system Xc(-) transporter attenuates autoimmune inflammatory demyelination. *J Immunol* 195:450–463.
26. Gmünder H, Eck HP, Benninghoff B, Roth S, Dröge W (1990) Macrophages regulate intracellular glutathione levels of lymphocytes. Evidence for an immunoregulatory role of cysteine. *Cell Immunol* 129:32–46.
27. Sha LK, et al. (2015) Loss of Nrf2 in bone marrow-derived macrophages impairs antigen-driven CD8(+) T cell function by limiting GSH and Cys availability. *Free Radic Biol Med* 83:77–88.
28. Angelini G, et al. (2002) Antigen-presenting dendritic cells provide the reducing extracellular microenvironment required for T lymphocyte activation. *Proc Natl Acad Sci USA* 99:1491–1496.
29. Falo LD, Jr, Kovacsovics-Bankowski M, Thompson K, Rock KL (1995) Targeting antigen into the phagocytic pathway in vivo induces protective tumour immunity. *Nat Med* 1:649–653.
30. Kvistborg P, et al. (2014) Anti-CTLA-4 therapy broadens the melanoma-reactive CD8+ T cell response. *Sci Transl Med* 6:254ra128.
31. Buchbinder EI, Desai A (2016) CTLA-4 and PD-1 pathways: Similarities, differences, and implications of their inhibition. *Am J Clin Oncol* 39:98–106.
32. Quezada SA, Peggs KS, Curran MA, Allison JP (2006) CTLA4 blockade and GM-CSF combination immunotherapy alters the intratumor balance of effector and regulatory T cells. *J Clin Invest* 116:1935–1945.
33. Siska PJ, et al. (2016) Fluorescence-based measurement of cystine uptake through xCT shows requirement for ROS detoxification in activated lymphocytes. *J Immunol Methods* 438:51–58.
34. Nabeyama A, et al. (2010) xCT deficiency accelerates chemically induced tumorigenesis. *Proc Natl Acad Sci USA* 107:6436–6441.
35. Atkuri KR, Herzenberg LA, Niemi AK, Cowan T, Herzenberg LA (2007) Importance of culturing primary lymphocytes at physiological oxygen levels. *Proc Natl Acad Sci USA* 104:4547–4552.
36. Persson B, Andersson A, Hultberg B, Hansson C (2002) The redox state of glutathione, cysteine and homocysteine in the extracellular fluid in the skin. *Free Radic Res* 36: 151–156.
37. Szatrowski TP, Nathan CF (1991) Production of large amounts of hydrogen peroxide by human tumor cells. *Cancer Res* 51:794–798.
38. Irani K, et al. (1997) Mitogenic signaling mediated by oxidants in Ras-transformed fibroblasts. *Science* 275:1649–1652.
39. Devi GS, et al. (2000) Free radicals antioxidant enzymes and lipid peroxidation in different types of leukemias. *Clin Chim Acta* 293:53–62.
40. Habtetsion T, et al. (2018) Alteration of tumor metabolism by CD4+ T cells leads to TNF-α-dependent intensification of oxidative stress and tumor cell death. *Cell Metab* 28:228–242.e6.
41. Hao S, et al. (2017) Cysteine dioxygenase 1 mediates erastin-induced ferroptosis in human gastric cancer cells. *Neoplasia* 19:1022–1032.
42. Dixon SJ, et al. (2014) Pharmacological inhibition of cystine-glutamate exchange induces endoplasmic reticulum stress and ferroptosis. *eLife* 3:e02523.
43. Tarangelo A, et al. (2018) p53 suppresses metabolic stress-induced ferroptosis in cancer cells. *Cell Rep* 22:569–575.

44. Dixon SJ, et al. (2012) Ferroptosis: An iron-dependent form of nonapoptotic cell death. *Cell* 149:1060–1072.
45. Panaretakis T, et al. (2009) Mechanisms of pre-apoptotic calreticulin exposure in immunogenic cell death. *EMBO J* 28:578–590.
46. Obeid M, et al. (2007) Calreticulin exposure dictates the immunogenicity of cancer cell death. *Nat Med* 13:54–61.
47. Mosely SI, et al. (2017) Rational selection of syngeneic preclinical tumor models for immunotherapeutic drug discovery. *Cancer Immunol Res* 5:29–41.
48. Qin W, et al. (2016) Generating mouse models using CRISPR-Cas9-mediated genome editing. *Curr Protoc Mouse Biol* 6:39–66.
49. Hogquist KA, et al. (1994) T cell receptor antagonist peptides induce positive selection. *Cell* 76:17–27.